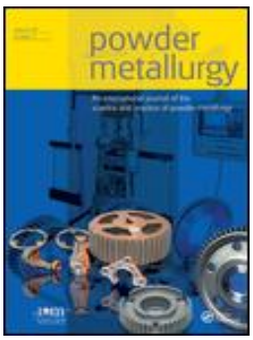

Powder Metallurgy

ISSN: 0032-5899 (Print) 1743-2901 (Online) Journal homepage: http://www.tandfonline.com/loi/ypom20

Microstructure and compression properties of in situ dual phase nanosized (TiB_2–Ti_5Si_3)/TiAl matrix composites fabricated by combustion synthesis and hot press consolidation

F. Qiu, Y. He, L. Zhu, S. L. Shu, W. Hu, C. H. Zhan & Q. C. Jiang

To cite this article: F. Qiu, Y. He, L. Zhu, S. L. Shu, W. Hu, C. H. Zhan & Q. C. Jiang (2015) Microstructure and compression properties of in situ dual phase nanosized (TiB_2–Ti_5Si_3)/TiAl matrix composites fabricated by combustion synthesis and hot press consolidation, Powder Metallurgy, 58:3, 235-240, DOI: 10.1179/1743290115Y.0000000010

To link to this article: http://dx.doi.org/10.1179/1743290115Y.0000000010

Published online: 23 Jul 2015.

Microstructure and compression properties of *in situ* dual phase nanosized ($TiB_2-Ti_5Si_3$)/TiAl matrix composites fabricated by combustion synthesis and hot press consolidation

F. Qiu[1], Y. He[1], L. Zhu[1], S. L. Shu[2], W. Hu[1], C. H. Zhan[1] and Q. C. Jiang*[1]

The dual phase nanosized (TiB_2–Ti_5Si_3)/TiAl composites were successfully fabricated using *in situ* method of combustion synthesis and hot press consolidation. The effects of proportions of the *in situ* dual phase nanoparticles (TiB_2 and Ti_5Si_3) on microstructures and compression properties of the composites were investigated. Compared with the monophase TiB_2 and Ti_5Si_3 particles, dual phase TiB_2–Ti_5Si_3 particles exhibit more obvious grain refinement effect. The grain size of TiAl alloy was refined from ~66 to ~12 μm with the the generation of dual phase TiB_2–Ti_5Si_3 particles. Moreover, the TiAl matrix composites reinforced with dual phase nanosized TiB_2–Ti_5Si_3 particles exhibit better comprehensive compression properties. When TiB_2:Ti_5Si_3 = 2:1[Σ(TiB_2 + Ti_5Si_3) = 4 vol.-%], the TiAl matrix composite has a high true fraction strain of 26.1%, a true yield strength of 761 MPa and an ultimate compression strength of 1647 MPa.

Keywords: Dual phase, Nanoparticles, *In situ*, TiAl matrix composites

Introduction

In recent years, with the development of the modern advanced aerospace and automotive applications technology, the TiAl intermetallics will be a candidate for high temperature applications in aerospace automobile industry owing to their low density, high specific strength and relatively good resistance to oxidation at service circumstance.[1,2] However, the properties of brittleness and low strength at room temperature are the main restrictions for their application.[3–5] In previous works, many researchers have tried to solve these problems by introducing the stiff and hard particle reinforcements to TiAl alloy, such as TiB, TiB_2, Al_2O_3, SiC, Ti_2AlC and Ti_5Si_3.[6–10] Nevertheless, the strength improvement by the addition of these particles was usually at the cost of the ductility. Recently, there are some reports that the dual phase ceramics have higher wear resistance and mechanical and electrical properties than the monolithic ceramics.[11–15] The TiB_2 and Ti_5Si_3 ceramic particles are the most frequently used reinforcing particles in the TiAl matrix composites since TiB_2 and Ti_5Si_3 have good orientation relationship and the habit plane with γ-TiAl.[16–18] However, the detailed effects of introducing hybrid TiB_2 and Ti_5Si_3 into the TiAl alloy are still unknown.

Many fabrication methods have been used to produce the TiAl matrix composites, such as combustion synthesis,[19,20] plasma arc melting process,[21] induction skull melting process[22] and hot isostatic pressing process.[23,24] In this study, the combustion synthesis plus hot press consolidation is used to fabricate the TiAl matrix composites reinforced with *in situ* dual phase nanosized TiB_2–Ti_5Si_3 particles. This method has the advantages of low energy requirement and cleaner particle/matrix interface, and the TiAl composites could be synthesised and densified simultaneously at lower temperatures. Moreover, the influence of the different ratios between TiB_2 and Ti_5Si_3 on the microstructures and compression properties of the composites are also investigated.

Experimental

The starting materials were made from commercial powders of titanium (99.5% purity, ~25 μm), aluminium (99% purity, ~74 μm), boron (98% purity, ~3 and 26 μm) and silicon (99.5% purity, ~25 μm). As shown in Table 1, sample A is a TiAl alloy, sample B is a 4 vol.-%TiB_2–TiAl composite (B powder with a particle size ~3 μm), sample C is a 4 vol.-%Σ (TiB_2:Ti_5Si_3 = 2:1)/TiAl composite, sample D is a 4 vol.-%Σ(TiB_2:Ti_5Si_3 = 1:1)/TiAl composite, sample E is a 4 vol.-%Σ(TiB_2:Ti_5Si_3 = 1:2)/TiAl composite, sample F is 4 vol.-%Ti_5Si_3–TiAl composite and sample G is a 4 vol.-%TiB_2–TiAl composite (B powder with a particle size ~26 μm). Elemental powder blends corresponding

[1]Key Laboratory of Automobile Materials, Ministry of Education, Department of Materials Science and Engineering, Jilin University, No. 5988 Renmin Street, Changchun 130025, China
[2]State Key Laboratory of Luminescence and Applications, Changchun Institute of Optics, Fine Mechanics and Physics, Chinese Academy of Sciences, Changchun 130012, China

*Corresponding author, email jqc@jlu.edu.cn

Published by Maney on behalf of the Institute
Received 10 February 2015; accepted 04 May 2015
DOI 10.1179/1743290115Y.0000000010

Table 1 Details of elements content and density of cylindrical powder compacts

Samples	Name	Density/g cm^{-3}	Relative density/%	Ti/g	Al/g	Si/g	B/g
A	TiAl	2.511±0.022	66.1±0.6	31.98	18.02	...	...
B	TiAl–4%TiB_2	2.508±0.025	65.5±0.7	32.10	17.17	...	0.73 (3 μm)
C	TiAl–4%(TiB_2:Ti_5Si_3 = 2:1)	2.513±0.023	65.7±0.6	32.14	17.18	0.20	0.48 (3 μm)
D	TiAl–4%(TiB_2:Ti_5Si_3 = 1:1)	2.532±0.026	66.2±0.7	32.16	17.18	0.30	0.36 (3 μm)
E	TiAl–4%(TiB_2:Ti_5Si_3 = 1:2)	2.520±0.021	65.9±0.5	32.18	17.18	0.40	0.24 (3 μm)
F	TiAl–4%Ti_5Si_3	2.541±0.024	66.5±0.6	32.21	17.20	0.59	...
G	TiAl–4%TiB_2	2.513±0.022	65.6±0.6	32.10	17.17	...	0.73 (26 μm)

to 'samples A–G' were mixed sufficiently by ball milling for 8 h and then cold pressed into cylindrical compacts using a stainless steel die. The powder compact with 28 mm diameter and ~36 mm height was placed in a graphite die, which was put into the self-made vacuum thermal explosion furnace (Fig. 1). The heating rate of the furnace was ~35 K min^{-1}, and the temperature was measured by Ni–Cr/Ni–Si thermocouples closed to the centre of the compact. When the temperature measured by the thermocouples suddenly rose rapidly, indicating that the compact should be ignited, the compact was quickly pressed just when it was in the soft state. The pressure (~30 MPa) was maintained for 30 s, and then, the product was cooled down to the ambient temperature.

The phase constituents of the composites were examined by X-ray diffraction (XRD, Rigaku D/Max 2500PC, Japan) with Cu K_α radiation. The morphologies of the ceramic particles were observed using a field emission scanning electron microscope (JSM-6700F, Japan). Deep etching was carried out using Keller's solution (2.5 mL HNO_3 + 1.5 mL HCl + 1 mL HF + 95 mL H_2O) for 5 min to reveal the TiB_2 and Ti_5Si_3 morphologies. Nanoparticles (TiB_2 and Ti_5Si_3) were carefully extracted from the sample using a mixed acid solution (20 mL HCl + 10 mL HF + 70 mL H_2O). The microstructures were investigated by scanning electron microscopy (SEM, Evo18, Carl Zeiss, Germany). The grain size was determined by the average line interception method. The density of the cylindrical powder compacts, TiAl alloy and its composites was measured by Archimedes' water immersion method.

The cylindrical specimens with a diameter of 3 mm and a height of 6 mm were used for compression tests; surfaces were polished place parallel. The uniaxial compression tests were carried out under a servohydraulic materials testing system (MTS 810, USA) with a strain rate of 10^{-4} s^{-1}.

Results and discussion

Phases identification and microstructure of composites

The XRD results of 'samples A–F' are shown in Fig. 2. Figure 2*a* shows that the sample without B and Si addition mainly consists of γ-TiAl and α_2-Ti_3Al phases. As shown in Fig. 2*b–f*, with the increase in addition value of B and Si elements, the peaks of the TiB_2 and Ti_5Si_3 phases begin to appear, and their intensities change with the different proportions of the synthesised TiB_2 and Ti_5Si_3 particles. The XRD results are consistent with the experimental design components. Figure 3 shows the microstructures of the 'samples A–F', and Fig. 4 shows their grain sizes. It can be seen that the grain size of TiAl is greatly refined by the synthesised ceramic particles. Moreover, the grain sizes of the TiAl matrix composites reinforced with dual phase nanoceramic particles (Fig. 3*c–e*) are more uniform, and the refinement effect of the dual phase nanoceramic particles (TiB_2 and Ti_5Si_3) is more obvious than that of the simplex nano-TiB_2 or nano-Ti_5Si_3 ceramics (Fig. 3*e–f*). As discussed in our previous work,[25] the nano-TiB_2 particles in the TiB_2/TiAl composite can refine the grain size of TiAl by obstructing the growth of the TiAl grain. While in the Ti_5Si_3/TiAl composite, the homogeneously distributed fine silicide particles in the TiAl grain can also act as preferred nucleation sites during recrystallisation, inducing fine grains in the TiAl composites. Hence, in the dual phase TiB_2–Ti_5Si_3/TiAl composites fabricated in this work, the abovementioned grain refinement mechanisms act simultaneously, indicating that the synthesised dual phase TiB_2–Ti_5Si_3 ceramics possess more obvious refinement effect. This is the reason why the dual phase TiB_2–Ti_5Si_3/TiAl composites exhibit finer grain sizes. As shown in Fig. 3*c*, sample C possesses the finest grain

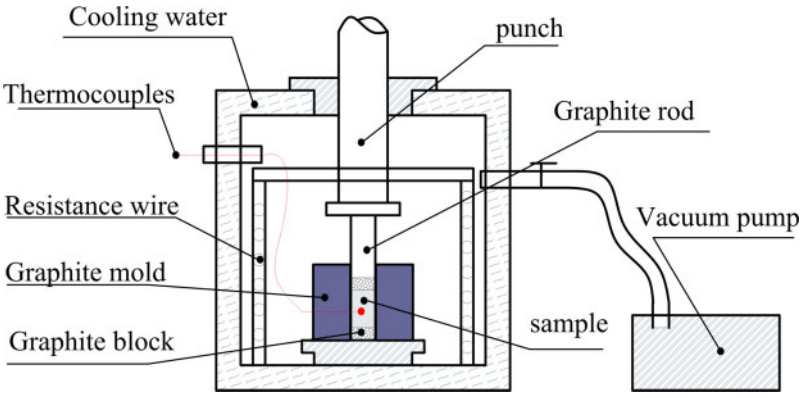

1 Schematic of equipment for combustion synthesis and hot press consolidation experiment

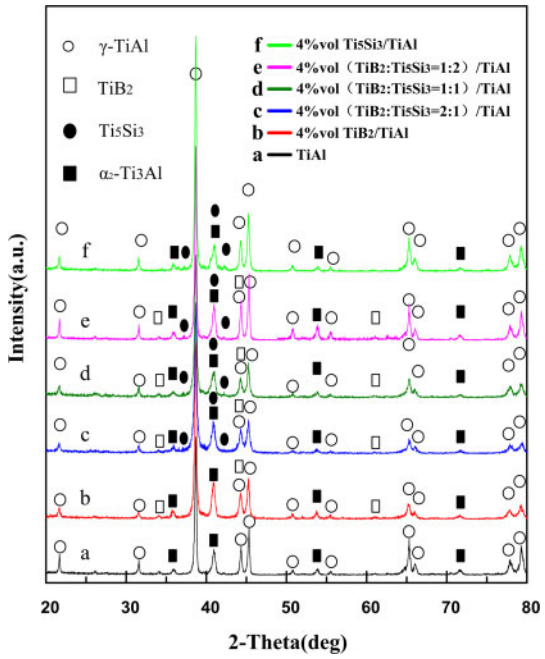

2 X-ray diffraction patterns of TiAl alloy and their composites

size. Its average grain size is ~12 μm, which is greatly smaller than those of TiAl alloy (~66 μm), TiB_2/TiAl composites (~20 μm) and Ti_5Si_3/TiAl composites (~25 μm).

Figure 5 shows the nanosized TiB_2, TiB_2–Ti_5Si_3 and Ti_5Si_3 particles extracted from the TiB_2/TiAl, TiB_2–Ti_5Si_3/TiAl and Ti_5Si_3/TiAl composites respectively. It can be seen that the sizes of the TiB_2–Ti_5Si_3 particles generated in the dual phase TiB_2–Ti_5Si_3/TiAl composites are smaller than those of TiB_2 and Ti_5Si_3 particles generated in the TiB_2/TiAl and Ti_5Si_3/TiAl composites.

Compression properties

Figure 6 shows the true stress–strain curves of 'samples A–F', and Table 2 summarises their compression properties and density. The figure shows that the yield strength σ^{y}_{ture} and ultimate compression strength σ^{UCS}_{ture} of 'samples B–F' are all higher than those of the TiAl alloy; thus, they are evidence that the strength of TiAl matrix composites is significantly enhanced by nanosized TiB_2 and Ti_5Si_3 particles. For the TiB_2/TiAl composite (sample B), it is significantly enhanced by nano-TiB_2 particles; the σ^{UCS}_{ture} of the 4 vol.-%TiB_2/TiAl composite is 414 MPa higher than that of the TiAl alloy, but the average fracture strain ε^{f}_{t} of the TiB_2/TiAl composite is weaker from 17.3 to 15.9%. In order to confirm whether the particle size of B has an effect on the mechanical properties of the composites, we have fabricated the TiB_2/TiAl composite (sample G) using B powder with a particle size ~26 μm and tested its compression properties. Compared with the TiB_2/TiAl composite (sample B) using B powder with a particle size ~3 μm (as shown in the Table 2), it can be seen that the size of B particle has little effect on the yielding strength, compression strength and fracture strain of the TiB_2/TiAl composites. As to the Ti_5Si_3/TiAl composite (sample F), the average ε^{f}_{t} of the TiAl alloy is significantly improved by nano-Ti_5Si_3 particles, the average ε^{f}_{t} is increased from 17.3 to 20.9% and the σ^{y}_{ture} and σ^{UCS}_{ture} are 613 and 1586 MPa respectively. These suggest that the TiAl alloy is better strengthened by the nano-TiB_2 ceramic particles, while the ductility of the TiAl alloy is improved more significantly by the nano-Ti_5Si_3 ceramic particles. Compared with the simplex nano-TiB_2/TiAl and simplex nano-Ti_5Si_3/TiAl composites, the dual phase nanoparticles (TiB_2 and Ti_5Si_3)/TiAl composites exhibit better compression properties. In addition, the reinforcement ability of dual phase nanoparticles (TiB_2 and Ti_5Si_3) is related to their proportions. As shown in Fig. 6*c*–*e*, the average σ^{y}_{ture} and σ^{UCS}_{ture} of the composites gradually increase with increasing content of TiB_2, and their

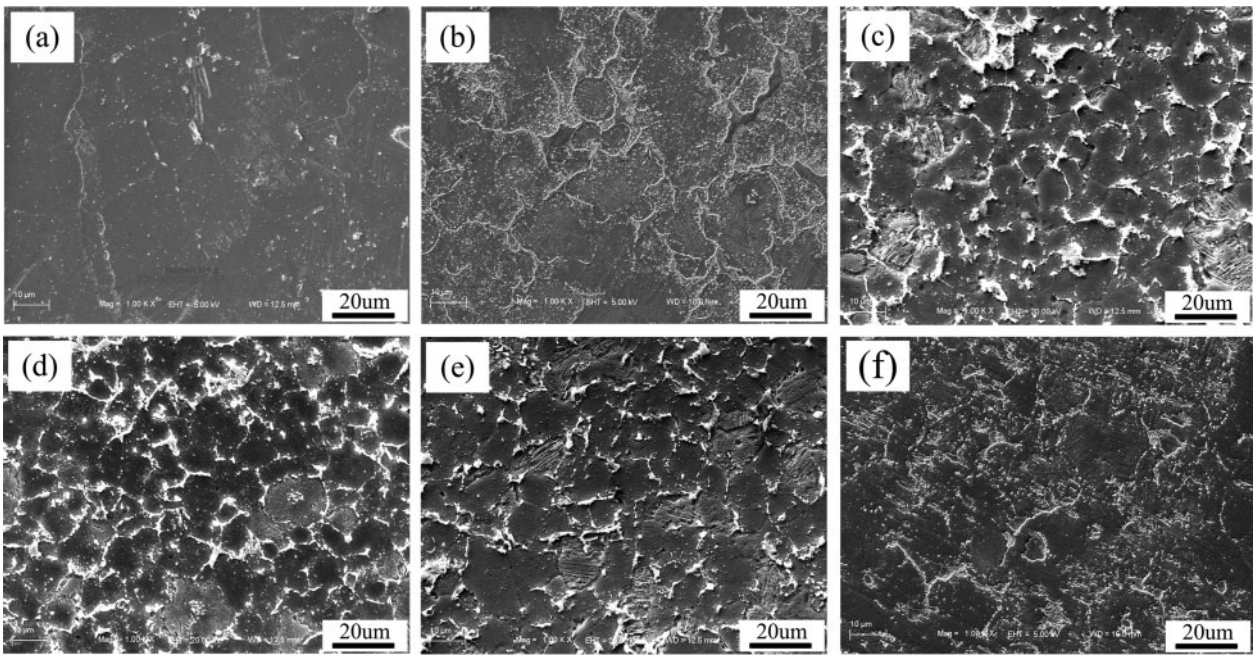

3 Microstructures of *a* TiAl alloy, *b* 4 vol.-%TiB_2/TiAl composites, *c* 4 vol.-%M(TiB_2:Ti_5Si_3 = 2:1)/TiAl composites, *d* 4 vol.-%M (TiB_2:Ti_5Si_3 = 1:1)/TiAl composites, *e* 4 vol.-%M(TiB_2:Ti_5Si_3 = 1:2)/TiAl composites and *f* 4 vol.-%Ti_5Si_3/TiAl composites

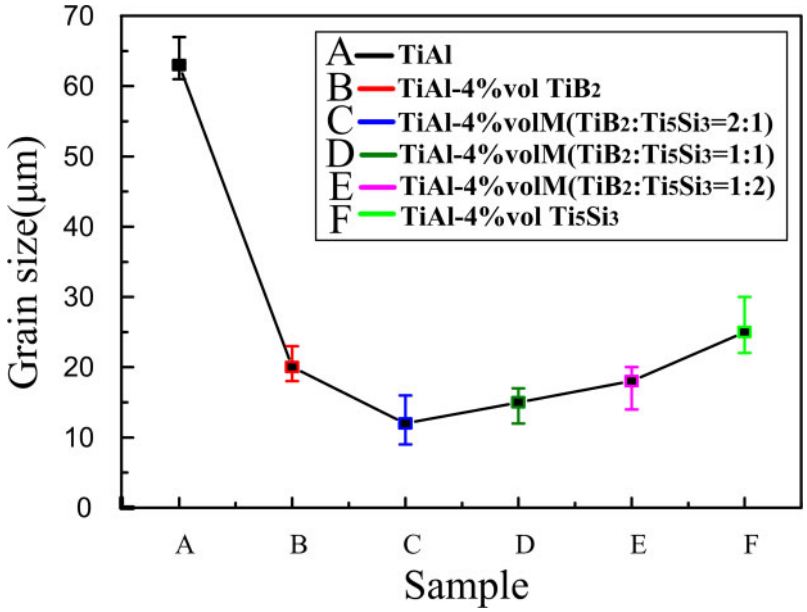

4 Grains size of γ-TiAl and α_2-Ti_3Al in TiAl alloy and their composites

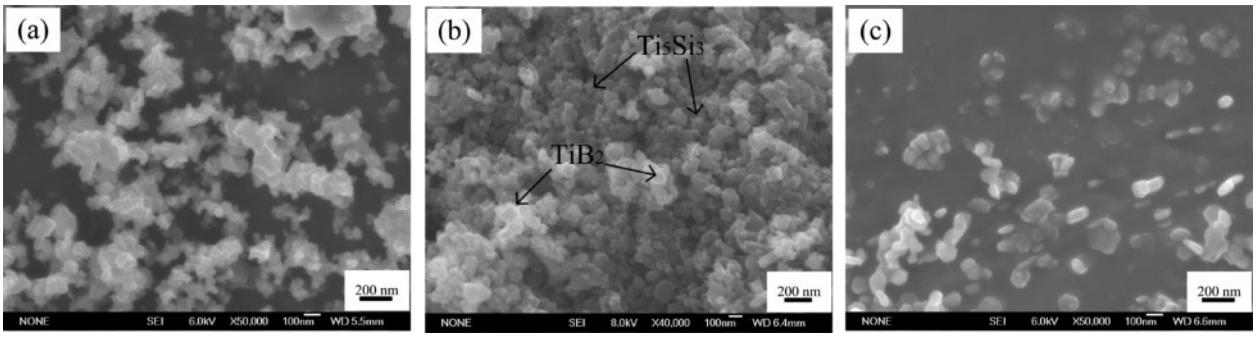

5 Images (FESEM) images of *a* extracted TiB_2 particles from 4 vol.-%TiB/TiAl composite, *b* extracted TiB_2 and Ti_5Si_3 particles from 4 vol.-%M(TiB_2:Ti_5Si_3 = 2:1)/TiAl composite and *c* extracted Ti_5Si_3 particles from 4 vol.-%Ti_5Si_3/TiAl composite

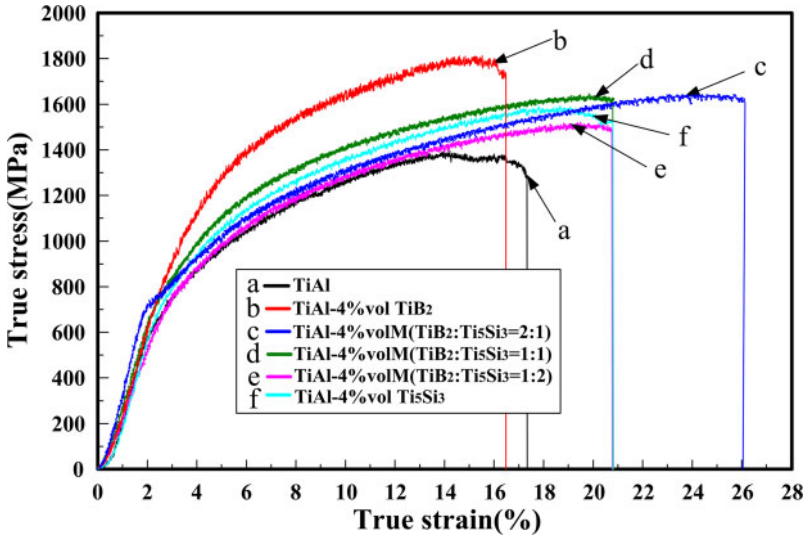

6 Compression true stress–strain curves of TiAl alloy and their composites

Table 2 Room temperature compression properties and density of TiAl alloy and its composites

Samples	Name	Density/g cm^{-3}	Relative density/%	σ^{y}_{true}/MPa	σ^{UCS}_{true}/MPa	ε^{f}_{true}/%
A	TiAl	3.697 ± 0.008	97.3 ± 0.2	465 ± 41	1415 ± 20	17.3 ± 0.43
B	TiAl-4% TiB_2	3.718 ± 0.011	97.1 ± 0.3	734 ± 5	1829 ± 17	15.9 ± 0.58
C	TiAl-4%(TiB_2:Ti_5Si_3 = 2:1)	3.707 ± 0.012	96.9 ± 0.3	761 ± 11	1647 ± 19	26.1 ± 0.75
D	TiAl-4%(TiB_2:Ti_5Si_3 = 1:1)	3.702 ± 0.011	96.8 ± 0.3	665 ± 9	1625 ± 15	20.7 ± 0.63
E	TiAl–4%(TiB_2:Ti_5Si_3 = 1:2)	3.678 ± 0.008	96.2 ± 0.2	625 ± 13	1510 ± 23	20.5 ± 0.31
F	TiAl–4%Ti_5Si_3	3.687 ± 0.007	96.5 ± 0.2	613 ± 7	1586 ± 7	20.9 ± 0.47
G	TiAl–4%TiB_2	3.722 ± 0.013	97.2 ± 0.3	743 ± 21	1833 ± 35	15.2 ± 0.37

average ε^{f}_{t} is almost the same as the Ti_5Si_3/TiAl composite. When the TiB_2:Ti_5Si_3 = 2:1[Σ(TiB_2 and Ti_5Si_3) = 4 vol.-%], the TiAl matrix composite (sample C) has the best compression properties, of which the ε^{f}_{t} is 26.1%, the σ^{y}_{ture} is 761 MPa and the σ^{UCS}_{ture} is 1647 MPa.

One of the most significant consequences of the generation of *in situ* nanoparticles is grain refinement, leading to the generation of a high volume density of grain boundaries to impede the movement and propagation of dislocations to adjacent grains, which is one reason for the strength enhancement of the composites. It is usually described by the Hall–Petch equation

$$\sigma_y = \sigma_0 + \frac{k_y}{d^{1/2}} \quad (1)$$

where σ_0 is the friction stress, d is the average grain diameter and k_y is the Hall–Petch slope. In our work, as shown in Fig. 4, the grain sizes of 'samples B–F' are smaller than that of TiAl alloy; this is one reason why their average σ^{y}_{ture} and σ^{UCS}_{ture} are all higher than those of the TiAl alloy. Moreover, 'sample C' with the smallest grain size among them possesses the highest σ^{y}_{ture}.

The other important consequence is the different proportions and distribution of nanoparticles (TiB_2 and Ti_5Si_3), which can enhance the composites by effecting the interaction between the dislocations and particles. Dispersion strengthening is governed by either the Orowan dislocation bypassing or the dislocation shearing mechanisms.[26] The critical shear stress τ_c to bypass a particle is defined as

$$\tau_c = A\frac{\mu b}{L}\left[\ln\left(\frac{\bar{D}}{r_0}\right) + B\right] \quad (2)$$

where L is the spacing between precipitates, D is the precipitate diameter, r_0 is the line energy cutoff radius defining the elastic dislocation nucleation size, A and B are coefficients and $\bar{D}$ is a quantity as $\bar{D} = (D^{-1} + L^{-1})^{-1}$. Mohles and Fruhstorfer had investigated the effect of randomness of the particle arrangement on the critical resolved shear stress by computer simulations.[27] They found that the fluctuations of obstacle density and the distances between the nearest neighbours had significant effects on the numerical value of L and $\bar{D}$, thereby reinforcing composites. In our work, the different proportions of dual phase nanoparticles (TiB_2 and Ti_5Si_3) have significant effects on randomness arrangements of particles, thereby strengthening composites by effecting the numerical value of L and $\bar{D}$. When TiB_2:Ti_5Si_3 = 2:1[Σ(TiB_2 and Ti_5Si_3) = 4 vol.-%], the dual phase nanoparticles (TiB_2 and Ti_5Si_3) are distributed more uniformly; thus, the TiAl matrix composite has the best combination of mechanical properties.

Conclusions

The dual phase nano-(TiB_2–Ti_5Si_3)/TiAl composites were successfully fabricated using the *in situ* method of combustion synthesis and hot press consolidation. With the generation of nanoceramic particles, there is an increase in average σ^{y}_{ture} and σ^{UCS}_{ture} of TiAl alloy due to the reinforcement of stiff nanoceramic particles and the grain refinement. Comparing with the nano-TiB_2/TiAl and nano-Ti_5Si_3/TiAl composites, the TiAl composites reinforced with dual phase nanosized TiB_2–Ti_5Si_3 particles exhibit better comprehensive compression properties, owing to the more significant influence of the dual phase nanosized TiB_2–Ti_5Si_3 particles on grain refinement. When TiB_2:Ti_5Si_3 = 2:1[ΣM(TiB_2 and Ti_5Si_3) = 4 vol.-%], the TiAl matrix composite has the best combination of compression properties among these TiAl matrix composites with a high true fraction strain of 26.1%, a true yield strength of 761 MPa and an ultimate compression strength of 1647 MPa.

Acknowledgement

This work is supported by the National Natural Science Foundation of China (NNSFC, grant no. 51171071), National Basic Research Program of China (973 Program, grant no. 2012CB619600), NNSFC (grant no. 50971065), the Research Fund for the Doctoral Program of Higher Education of China (grant no. 20130061110037), the Innovation Experimental Training Project of Jilin University in 2014 (grant no. 2014A43152) and the Project 985 – High Properties Materials of Jilin University.

References

1 J. L. Immarigeon, R. T. Holt, A. K. Koul, L. Zhao, W. Wallace and J. C. Beddoes: 'Lightweight materials for aircraft applications', *Mater. Charact.*, 1995, **35**, 41–67.
2 D. Legzdina, I. M. Robertson and H. K. Birnbaum: 'Oxidation behavior of a simplex phase γ-TiAl alloy in low-pressure oxygen and hydrogen', *Acta Mater.*, 2005, **53**, 601–608.
3 S. Nishikiori, K. Matsuda and Y. G. Nakagawa: 'Microstructural effects on tensile properties of cast TiAl-Fe-V-B alloy', *Mater. Sci. Eng. A*, 1997, **A239-A240**, 592–599.
4 T. Izumi, T. Yoshioka, S. Hayashi and T. Narita: 'Oxidation behavior of sulfidation processed TiAl-2 at.% X (X=V, Fe, Co, Cu, Nb, Mo, Ag and W) alloys at 1173 K in air', *Intermetallics*, 2001, **9**, 547–558.
5 R. Bohn, T. Klassen and R. Bormann: 'Room temperature mechanical behavior of silicon-doped TiAl alloys with grain sizes in the nano- and submicron-range', *Acta Mater.*, 2001, **49**, 299–311.
6 M. L. VanMeter, S. L. Kampe and L. Christodoulou: 'Mechanical properties of near-γ titanium aluminides reinforced with high volume percentages of TiB', *Scr. Mater.*, 1996, **34**, 1251–1256.
7 C. L. Yeh and R. F. Li: 'Formation of TiAl-Ti_5Si_3 and TiAl-Al_2O_3 in situ composites by combustion synthesis', *Intermetallics*, 2008, **16**, 64–70.

8 J. Liu, J. C. Feng and Y. Y. Qian: 'Interface structure and formation mechanism of diffusion-bonded joins of SiC ceramic to TiAl-based alloy', *Scr. Mater.*, 2000, **43**, 49–53.

9 O. N. Senkov, M. Cavusoglu and F. H. Froes: 'Synthesis and characterization of a $TiAl/Ti_5Si_3$ composite with a submicrocrystalline structure', *Mater. Sci. Eng. A*, 2001, **A300**, 85–93.

10 P. Novák, T. Popela, J. Kubásek, J. Šerák, D. Vojtěch and A. Michalcová: 'Effect of reactive sintering conditions on microstructure of in situ titanium aluminide and silicide composites', *Powder Metall.*, 2011, **54**, (1), 50–55.

11 Y. F. Yang and Q. C. Jiang: 'Reaction behaviour, microstructure and mechanical properties of TiC-TiB_2/Ni composite fabricated by pressure assisted self-propagating high-temperature synthesis in air and vacuum', *Mater. Des.*, 2013, **49**, 123–129.

12 Q. Guo, D. L. Sun, L. T. Jiang, G. H. Wu and G. Q. Chen: 'Residual microstructure and damage geometry associated with high speed impact crater in Al_2O_3 and TiB_2 particles reinforced 2024 Al composite', *Mater. Charact.*, 2012, **66**, 9–15.

13 J. J. Liu and Z. D. Liu: 'An experimental study on synthesizing TiC-TiB_2-Ni composite coating using electro-thermal explosion ultra-high speed spraying method', *Mater. Lett.*, 2010, **64**, 684–687.

14 J. B. Lu, S. L. Shu, F. Qiu, Y. W. Wang and Q. C. Jiang: 'Compression properties and abrasive wear behavior of high volume fraction TiCx-TiB_2/Cu composites fabricated by combustion synthesis and hot press consolidation', *Mater. Des.*, 2012, **40**, 157–162.

15 Y. F. Yang and Q. C. Jiang: 'Effect of TiB_2/TiC ratio on the microstructure and mechanical properties of high volume fractions of TiB_2/TiC reinforced Fe matrix composite', *Int. J. Refract. Met. Hard Mater.*, 2013, **38**, 137–139.

16 D. Gosslar, R. Günther, U. Hecht, C. Hartig and R. Bormann: 'Grain refinement of TiAl-based alloys: the role of TiB_2 crystallography and growth', *Acta Mater.*, 2010, **58**, 6744–6751.

17 F. S. Sun and F. H. Sam Froes: 'Precipitation of Ti_5Si_3 phase in TiAl alloys', *Mater. Sci. Eng. A*, 2002, **A328**, 113–121.

18 R. Yu, L. L. He, J. T. Guo, H. Q. Ye and V. Lupinc: 'Orientation relationship and interfacial structure between ζ-Ti_5Si_3 precipitates and γ-TiAl intermetallics', *Acta Mater.*, 2000, **48**, 3701–3710.

19 C. L. Yeh and S. H. Su: 'In situ formation of TiAl-TiB_2 composite by SHS', *J. Alloys Compd*, 2006, **407**, 150–156.

20 Y. Jiang, Y. H. He, B. Y. Huang, J. Zou, H. Huang, N. P. Xu and C. T. Liu: 'Criterion to control self-propagation high temperature synthesis for porous Ti-Al intermetallics', *Powder Metall.*, 2011, **54**, (3), 404–407.

21 A. Hirose, M. Hasegawa and K. F. Kobayashi: 'Microstructures and mechanical properties of TiB_2 particle reinforced TiAl composites by plasma arc melting process', *Mater. Sci. Eng. A*, 1997, **A239-A240**, 46–54.

22 H. Z. Niu, S. L. Xiao, F. T. Kong, C. J. Zhang and Y. Y. Chen: 'Microstructure characterization and mechanical properties of TiB_2/TiAl in situ composite by induction skull melting process', *Mater. Sci. Eng. A*, 2012, **A532**, 522–527.

23 H. B. Yu, D. L. Zhang, Y. Y. Chen, P. Cao and B. Gabbitas: 'Synthesis of an ultrafine grained TiAl based alloy by subzero temperature milling and HIP, its microstructure and mechanical properties', *J Alloys Compd*, 2009, **474**, 105–112.

24 W. Zhang, Y. Liu, B. Liu and B. Y. Huang: 'Comparative assessment of microstructure and compressive behaviours of PM TiAl alloy prepared by HIP and pseudo-HIP technology', *Powder Metall.*, 2011, **54**, (2), 133–141.

25 S. L. Shu, B. Xing, F. Qiu, S. B. Jin and Q. C. Jiang: 'Comparative study of the compression properties of TiAl matrix composites reinforced with nano-TiB_2 and nano-Ti_5Si_3 particles', *Mater. Sci. Eng. A*, 2013, **A560**, 596–600.

26 D. J. Bacon, U. F. Kocks and R. O. Scattergood: 'The effect of dislocation self-interaction on the Orowan stress', *Philos. Mag. A*, 1973, **28A**, 1241–1263.

27 V. Mohles and B. Fruhstorfer: 'Computer simulations of Orowan process controlled dislocation glide in particle arrangements of various randomness', *Acta Mater.*, 2002, **50**, 2503–2516.